Light Metals 2013 *Edited by: Barry Sadler*
TMS (The Minerals, Metals & Materials Society), 2013

Light Metals 2013

ALUMINUM REDUCTION TECHNOLOGY

Fundamentals: Chemistry

SESSION CHAIR
Arne Ratvik
NTNU
Trondheim, Norway

Light Metals 2013 *Edited by: Barry Sadler*
TMS (The Minerals, Metals & Materials Society), 2013

COMPOSITION AND THERMAL ANALYSIS OF CRUST FORMED FROM INDUSTRIAL ANODE COVER

Qinsong Zhang[1,2], Mark P. Taylor[1], John J.J. Chen[1], David Cotton[1], Tania Groutzo[1], Xiaodong Yang[2]
1. Light Metals Research Centre, Department of Chemical and Materials Engineering, The University of Auckland, Private Bag 92019, Auckland, New Zealand
2. Shenyang Aluminium & Magnesium Engineering & Research Institute Co. Ltd, Shenyang, Liaoning, 110001. P.R. China

Keywords: cryolite, chiolite, crust, anode cover, composition, liquidus temperature

Abstract

When the anode cover is heated up in the reduction cell, the crust formation from the anode cover commences at the bottom and the process is driven by thermo-chemical processes. It is important to study the composition and thermal stability properties of the crust in order to understand the mechanisms of crust formation and deterioration. Several crust pieces were taken from industrial prebaked anode cells. A number of vertical crust sections were sampled from these pieces, and each section was analyzed for composition and phase change temperature. Results show that the bottom layer is enriched in cryolite, consistent with results published in the literature. The upper region was found to contain more chiolite. Crushed bath-based anode crust has higher CR than alumina based anode crust. The melting of chiolite in the crust leaves substantial macro-porosity there, which contributes to the absorption of $NaAlF_4$ and the penetration of bath through it. The formation conditions of crystalline crust were discussed.

Introduction

In industrial aluminium reduction cells, smelter alumina or crushed bath/alumina granular mixtures are used to cover the anode and the central channel to protect anodes from air burn, to absorb fluoride fumes, and to control heat loss. Inside the anode cover, transition phase of alumina is transformed to alpha alumina at about 800 °C in the presence of fluorides; and crushed bath consolidates through partial fusing of the bath particulates to each other. Thus at the bottom of the cover, a crust is slowly being formed consisting of alumina particles embedded in a mixture of frozen and liquid bath.

Johnston and Richards [1] made synthetic alumina based crust samples in the laboratory. Rye et al. [2] did similar work as well. Analysis of the bath phase in the crust in these studies showed that the top zone of the crust is far more acidic than the lower crust zone, the bath ratio in the crust is much lower than their corresponding electrolyte.

A few investigations have been done about industrial crust formed from crushed bath/alumina mixtures. Liu et al. [3] gave some results of the composition and thermal analysis of crust samples taken from industrial cells. Crusts in these studies consisted of three major phases: alpha alumina, chiolite and cryolite. The bottom layer of the crusts has a higher bath ratio more similar to the bulk electrolyte compared to the upper layers. Similar compositions of industrial crusts were obtained by Groutso et al. [4], and in this study the intimate encapsulation of chiolite and corundum phases was found to create a material of extreme hardness and toughness.

Heat balance and bath mass balance both have effects on crust formation, which is also strongly influenced by the composition and thermal properties of the crust. In the present work, composition and thermal property of several types of industrial crust were studied to further understand about the process of crust formation.

Experimental Materials

7 pieces of crust (designated as Crust A, B, C, D, E, F, and G) were taken from industrial prebaked anode reduction cells three months after start-up. These crust pieces were selected because of their typical features. Some crust pieces have clearly distinguishable features between the lower and the upper part. While the lower part is crystalline, the portion above the crystalline crust is not and will be referred to sintered crust in this paper.

Sintered crusts are differentiated by raw anode cover material. There are three types of sintered crusts: alumina based crust (Crust C), crushed bath/alumina blend crust (Crust A and D) and crushed bath-based crust (Crust B).

Based on the difference in appearance and shape, crystalline crusts are sorted into the three following types, as shown in Figure 1. Type I crystalline crust has nearly uniform thickness. Type II crystalline crust is made up of laminar layers. The thickness of each layer is approximately 1~5 mm. Type III crystalline crust has an irregular surface and stalactitic shape crystal.

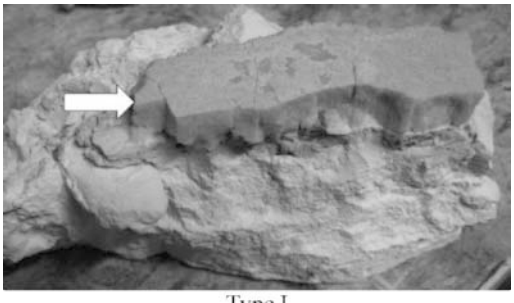

Type I

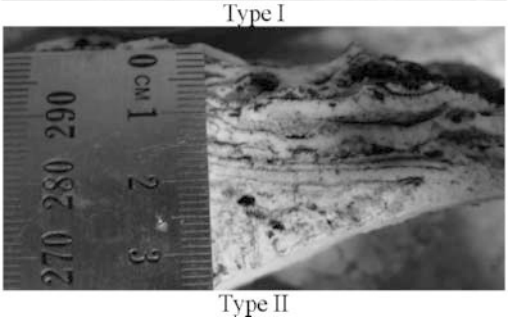

Type II

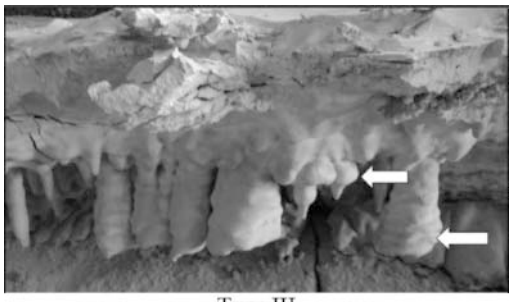

Type III

Figure 1. View of different types of crystalline crust (indicated by arrow)

The apparent densities of crystalline crust and sintered crust were measured by the buoyancy method (see Table I). The macro porous sections were excluded from the density measurement.

Formed from crushed bath/alumina mixture anode cover material, sintered crusts of Crust A and D have higher apparent density (about 2.9 g/cm^3) than either alumina based Crust *C* (1.66 g/cm^3) or crushed bath based Crust B (2.60 g/cm^3).

Each crust piece is divided vertically into a number of sections starting from the crystalline crust at the bottom. One or two samples are taken from each section.

Table I. Property of crust pieces

Crust	Life (days)	Crystalline crust			Sintered crust	
		Type	Thickness (cm)	Apparent Density (g/cm^3)	Thickness (cm)	Apparent Density (g/cm^3)
A	28	I	1.5	2.53	3.0	2.91
B	24	I	2.5～3.0	2.58	6.0	2.60
C	28	I	1.3	2.46	6.0	1.66
D	5	III	0.1～0.2	--	6.0	2.90
E	13	II	2.0～4.0	2.46	--	--
F	28	III	0.5～1.0	2.16	--	--
G	11	--	--	--	--	2.34

Results and Discussion

Results Analysis

The composition and thermal analysis results of all sections are given in Table II. The crust samples are further classified based on their physical position as measured from the bottom surface of sintered crust.

Table II. Results of chemical composition and thermal analysis

sample	From bottom surface of sintered crust (cm)	Composition by XRD Rietveld refinement (w %)										CR from XRD result	Phase change temperature by DTA				w % Al_2O_3 by Oxygen Analyzer
		Major phases				Stoichiometry concentration							Cryolite α->β transition °C		Crystal <-> Liquid transition °C		
		α-Al_2O_3	γ-Al_2O_3	Cryolite	Chiolite	NaF	AlF_3	LiF	KF	MgF_2	CaF_2		Heating	Cooling	Heating	Cooling	
A1	I	1.4	0.0	71.3	4.6	52.4	39.9	1.4	0.6	1.4	2.0	2.63	550	546	990	978	0.34
A2	0.0	15.9	0.0	54.6	5.4	43.2	34.1	1.3	0.7	2.0	1.9	2.54	552	543	955	950	
A3	1.0	28.8	0.0	50.8	6.7	37.0	28.9	0.2	0.9	1.0	2.2	2.56		543	956	948	25.83
A4	1.5	24.0	0.0	36.2	6.4	36.6	31.2	2.3	1.1	2.5	1.6	2.35			916	917	
A5	2.0	30.2	0.0	34.8	4.2	33.7	28.2	1.6	0.9	3.5	1.3	2.39		575	928	920	
A6	2.5	29.3	0.0	29.8	5.7	33.1	28.8	2.0	1.2	3.7	1.3	2.30	551		925		
A7	3.0	10.2	0.0	27.8	8.9	39.6	36.9	3.4	2.1	4.5	2.2	2.15		580		878	
B1	I	1.1	0.0	73.1	4.1	53.1	40.0	1.5	0.5	1.0	1.9	2.65	550	545	990	984	0.49
B2	0.0	2.8	0.0	64.4	3.3	50.1	39.0	1.6	1.3	2.6	1.8	2.57	550	545	956	950	2.42
B3	1.0	2.7	0.0	73.3	6.7	52.9	39.7	1.0	0.8	1.2	1.1	2.66	550	547	954	954	
B4	2.0	2.8	0.0	67.1	3.2	50.9	39.2	1.8	1.2	1.5	1.8	2.60			944	925	
B5	2.0	2.9	0.0	65.3	2.5	50.1	38.9	1.8	1.4	1.7	2.1	2.57	542	574/535	945	931	
B6	3.0	9.1	0.0	64.6	7.1	48.3	37.1	1.1	1.3	1.2	1.2	2.60		578	938	932	
B7#	4.0	7.1	0.0	52.9	8.7	43.1	37.1	0.4	2.9	1.7	5.2	2.32		573	935	925	
B8#	5.0	6.4	4.4	51.7	9.1	43.5	36.2	0.8	2.6	2.7	2.4	2.40			928	923	11.81
B9#	6.0	8.8	7.5	41.9	13.9	39.3	34.5	0.5	2.2	3.1	2.8	2.28		570/540	936	931	
C1	I	1.5	0.0	70.4	5.1	52.1	39.8	1.2	0.8	1.8	1.9	2.62			995	985	0.24
C2	0.0	28.7	0.0	46.0	6.0	36.5	29.0	0.8	1.5	1.8	1.2	2.52			934	922	
C3	2.0	33.8	0.0	36.5	6.8	31.8	26.8	0.7	1.5	2.1	2.1	2.37			930	917	31.60
C4	4.0	33.4	0.0	36.1	6.5	31.9	27.0	0.8	1.7	2.2	2.0	2.36			915	912	
C5	6.0	51.7	0.0	11.3	14.6	20.9	20.9	0.8	1.0	2.9	1.2	1.99		570	816		47.14
D1	0.0	22.5	0.0	54.7	5.0	40.4	31.1	0.3	1.3	2.3	1.4	2.60	543	580/545	952	948	
D2	2.0	22.2	1.4	40.3	7.2	36.1	30.7	0.7	2.0	3.3	2.4	2.35			930	925	
D3	3.0	25.6	1.2	39.7	5.7	35.1	29.4	1.0	2.0	2.8	1.8	2.39			917	911	27.49
D4	4.0	23.2	2.2	36.9	6.7	35.0	30.1	1.3	2.1	2.7	2.2	2.32			865	865	
D5	6.0	20.4	9.6	23.5	5.5	29.3	27.7	1.2	3.4	4.6	2.6	2.12				820	27.81
E1	II	2.9	0.0	60.6	7.6	47.6	38.8	0.3	2.3	3.0	3.4	2.45		577	931	926	4.85
F1	III	2.0	0.0	67.6	6.6	50.3	39.3	0.4	1.3	2.5	2.7	2.56		535	968	960	
F2	III (stalactitic)	3.1	0.0	53.5	4.6	48.9	39.6	3.2	1.4	2.4	0.9	2.47			927	927	2.93
G1#	bottom	1.5	0.0	34.4	41.6	46.3	44.9	0.8	3.0	1.8	1.2	2.06	725*	678*	950	950	
G2	top	1.7	0.0	4.7	80.1	44.4	51.1	1.2	0.4	0.6	0.4	1.74	725*	680*		905	1.69

I,II,III means Crystalline crust type . #: Macro-porous. *: Chiolite melting or eutectic temperature

1) Composition

The composition of all samples was examined by X-ray powder diffractometer (XRD). XRD results indicate that crusts consist of three major phases: alpha alumina, cryolite, and chiolite. There were quite a number of other phases detected in the present crusts such as AlF_3, K_2NaAlF_6, $LiNa_2AlF_6$, CaF_2, Na_2LiAlF_6, $Na_2Ca_3Al_2F_{14}$, Na_2MgAlF_7, $NaCaAlF_6$, and $NaF{\cdot}1.5CaF_2{\cdot}AlF_3$. Of these phases K_2NaAlF_6 and $LiNa_2AlF_6$ existed in most of the present samples. For simplicity, the concentrations of NaF, AlF_3, LiF, KF, MgF_2, and CaF_2 have been calculated where necessary from the stoichiometry of the phases listed above. Multiphase Rietveld refinements of XRD data were done for all samples by using Fullprof software. Alumina concentrations in several samples were measured quantitatively by LECO Oxygen Analyzer.

(1) Effects of preferential crystallization of penetrated bath and decomposition of $NaAlF_4$

The lower sections of the crusts have higher cryolite concentration and Cryolite Ratio (CR = mol NaF/mol AlF_3) than the upper sections. Especially with the crystalline crust, this higher cryolite concentration and higher CR is even more pronounced. The amount of chiolite phase increases from the bottom of the crust to the top. Similar trends of cryolite and chiolite vertical concentration distributions have been reported by Liu et al [3] and Groutzo et al [4].

This uneven composition distribution is mainly caused by following: (i) During crust formation the cryolite component preferentially crystallizes from the penetrating bath at the lower part of the crust. Thus, the bath liquid phase moving upward becomes increasingly enriched in AlF_3 and other additives. (ii) $NaAlF_4$ decomposes to solid chiolite and AlF_3 below 680 °C which results in the enrichment of chiolite at the top of the crust.

(2) Effect of chiolite melting

Sample G2 at the top of Crust G contains the highest chiolite concentration which is more than 80 %, see Table II. Sample G1, at the bottom of Crust G, has millimetre scale macro pores, see Figure 2, and contains less chiolite but more cryolite than sample G2. The melting of chiolite at the bottom appears to have made it porous. This also implies that the starting cover material of Crust G was highly enriched in chiolite.

Figure 2. View of Crust G bottom

As shown in Figure 3, the top of Crust B is macro porous, below which there is no macro pore. One possible reason for this is that the chiolite component in Crust B melted and dripped down to bath, leaving macro pores there at an early stage, as in the bottom of Crust G. Once the bulk bath contacted the bottom of the crust, the bath liquid penetrated from the bottom and filled the voids gradually. The isotherm then moves upwards correspondingly and causes melting of the chiolite component at locations where the crust is above about 725 °C.

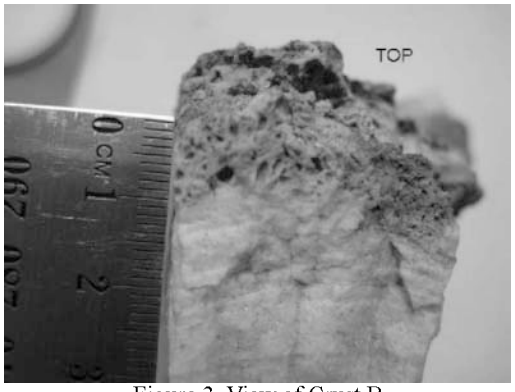

Figure 3. View of Crust B

(3) Effect of alumina concentration

The overall cryolite concentration and CR in crushed bath based Crust B are higher than alumina enriched crust pieces. This implies that in Crust B the high acidic liquid phase migrated downwards and eventually fall into the bulk bath. The reason why it did not happen in alumina enriched crust pieces is probably this: The initial liquid bath penetrating into the crust was usually not saturated with alumina. Dissolution of alumina into the bath absorbs large amount of heat. In alumina enriched crust, most liquid bath was cooled and solidified fast. In addition, the interlocking network of alpha alumina prevented the remain liquid bath from moving downwards.

2) Phase Change Temperatures

Laboratory tests were carried out on some samples to determine the phase change temperature by the Differential Thermo-Analysis (DTA) method. The reference material was alpha alumina. The samples were heated to 1020 °C and then cooled down. Both heating and cooling curves were recorded. The heating and cooling rates were both 1 °C /min.

Several kinds of phase change peaks are observed from the DTA curves. (1) Peak of cryolite crystallisation <–> liquid transition was detected for most samples. The onset temperature from the cooling curve was taken as the liquidus point of the crust sample. The peak temperature from heating curve was taken as the melting temperature of the whole, heterogeneous solid crust sample. However, crust samples with high alumina concentration melt partly with some alumina still in solid phase under 1020 °C. For these samples, the peak temperature is actually the pseudo-eutectic temperature of cryolite and alumina. (2) A Peak of cryolite α <–> β solid phase transition around 530 to 580 °C was detected, although the peak for the decomposition of Na_2LiAlF_6 to Na_3AlF_6, LiF, and AlF_3 at 543 °C might be detected as well [5,6]. (3) A Peak of incongruent melting of chiolite ($Na_5Al_3F_{14}$(s) +

$Al_2O_3(s) = Na_3AlF_6(s) + Liquid$) around 725 °C [6] was detected from heating curve, while the peak for the eutectic reaction ($L_E = Na_5Al_3F_{14}(s) + Al_2O_3(s) + AlF_3(s)$) around 680 °C [6] was detected from the cooling curve in chiolite enriched samples G1 and G2.

The melting and liquidus temperature of crystalline samples is about 980 to 990 °C. As the concentration of additives increase, the liquidus and melting temperature are depressed. Generally, the crust with lower CR has lower liquidus and melting temperature.

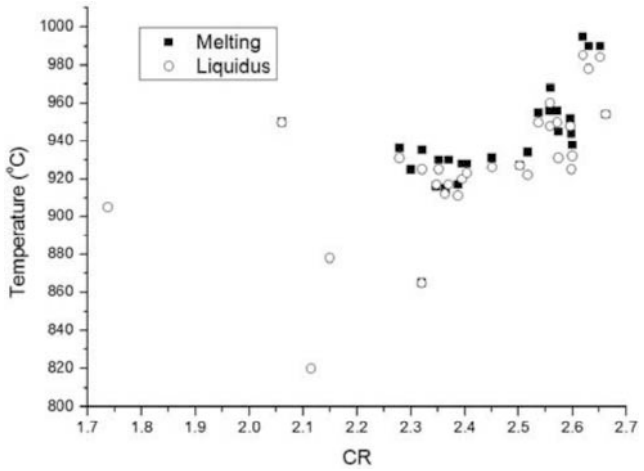

Figure 4. The influence of CR on the liquidus and melting point

Crust Formation

1) Sintered Crust Formation

The sintered crust formation mechanism has been described by previous researchers [1-3,7,8]. The evolution of sintered crust is shown in Figure 5. Melting of the crust bottom lead to an air gap between the bulk bath and the crust, at which point the liquid bath stops penetrating into the crust. At the same time, the crust is still able to contact the bath over the duration of the anode rota due to bath level variation for the period relevant for the crust formation process depicted in Figure 5. Extra bath was added to the cell by the smelter technician when the bath level was considered to be lower than normal. In addition, the crust moves gradually downwards with the anode due to continuous anode consumption and the adjustment for voltage.

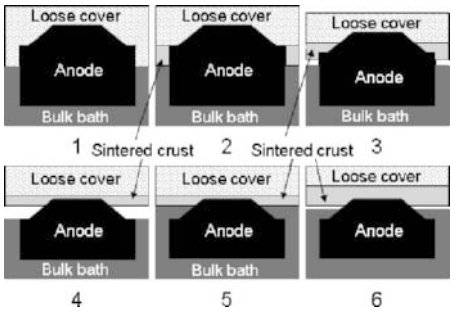

Figure 5. Sintered crust formation. 1)Anode cover added, 2)Sintered crust formed, 3-4)Crust bottom melted. 5) Bath level increased 6) Crust thickness increased until crust bottom melts again

The more contact between the bulk bath and the crust, the more bath liquid penetrated into the crust. In fact, this transfer of bath liquid is one of the reasons for the consequent reduction of bath level. Thus the liquid proximity and penetration into the crust has a profound affect on the crust composition, and visa versa.

2) Crystalline Crust Formation

The morphology of some crust pieces were observed by using the optical microscope. Type I crystalline crust is made of mainly macrocrystalline texture (crystals are visible to the naked eye), while type II crust is of microaphanitic texture (crystals are too small to be recognized under the microscope), and type III is of microcrystalline texture (crystals are small enough to be visible only under the microscope), as shown in Figure 6, in which a1 and a2 are for Sample B1 (Type I crust), b1 and b2 are for sample F2 (Type III crust), and c1 and c2 are for sample E1 (Type II crust). The cooling rate during crystallization accounts for the contrast among them. When the cooling rate is slow, slow nucleation rate and high growth rate lead to the formation of macrocrystalline crystal, a1&a2 in Figure 6. When cooling rate is fast, microcrystalline crystal is formed due to high nucleation rate and slow growth rate, c1&c2 in Figure 6. When cooling rate is too fast, crystal nucleation and growth is stunted and microaphanitic crystal is formed, b1&b2 in Figure 6.

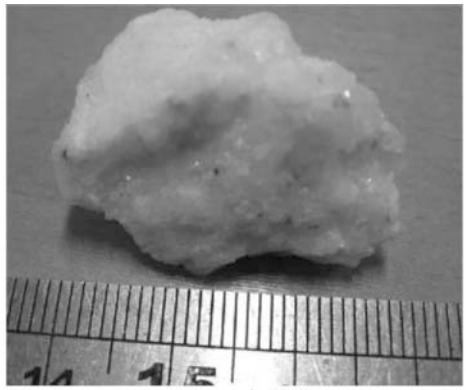

a1 (sample B1)

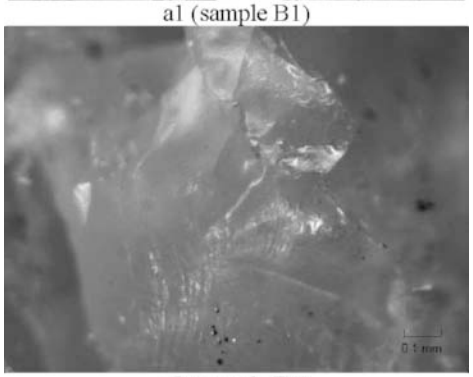

a2 (sample B1)

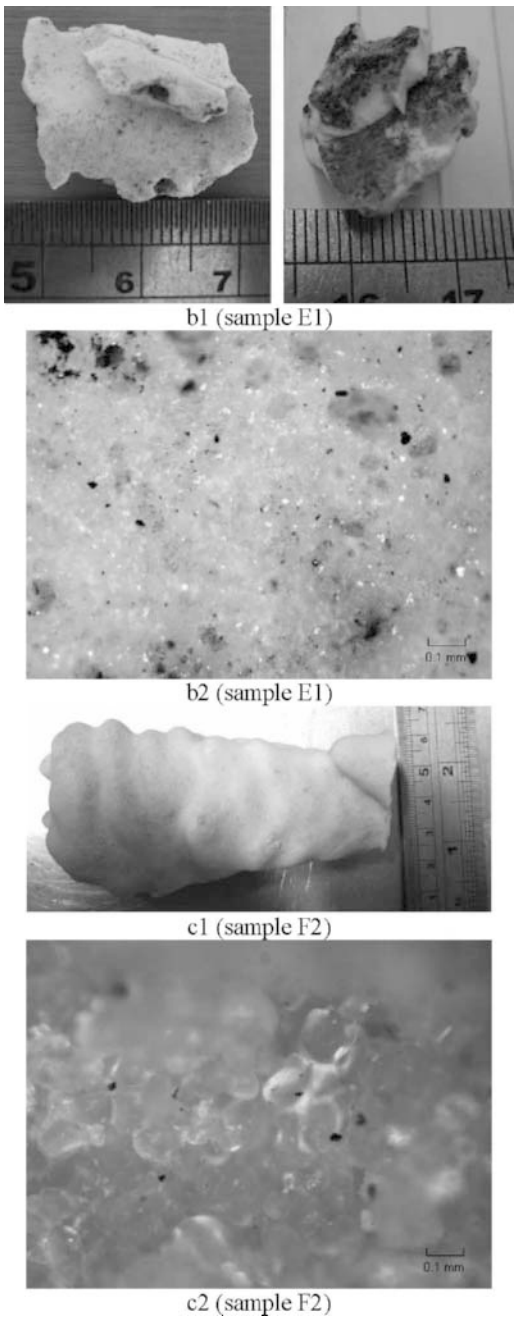

Figure 6. Surface morphology of crystalline crust. (a1,b1,c1 by camera; a2,b2,c2 by optical microscope)

It is obvious that the crystalline crust was crystallized from the bulk bath. The top insulation and the bath superheat were both crucial for the formation of crystalline crust. Crystalline crust was more likely formed where insulation was poor. It might not exist in some cell at all, or they might occur at certain localised positions.

(1) Type I crystalline crust formation

During the later stages of the anode rota, the bottom of the sintered crust melts and its thickness is reduced, as depicted in Figure 7, 1-2. If the bath level was increased sufficiently to make contact with the crust and at the same time the bath superheat was not quite high enough, the formation of type I crystalline crust is most likely to be expected, as shown as 3-4 in Figure 7.

Under the condition that the bulk bath is in full contact with the crust, heat will transfer from the bath to the crust by convection and conduction rather than radiation, and a temperature gradient will exist in the bath zone adjacent to the solid boundary. The macrocrystalline crystal is expected to form slowly by fractional crystallization when the bath temperature is only a few degrees below the liquidus point. The rest of the liquid with high additives concentration will diffuse to the bulk bath leaving cryolite enriched macrocrystalline crystal on the bottom of the crust.

The formation of macrocrystalline crystal starts from the boundary where the temperature is lower than the bath. The boundary moves downwards, and the crystalline crust increases its thickness with time. The formation of crystalline crust will cease when the crust provides sufficient insulation to the flow of heat. These are depicted in 4-5 in Figure 7.

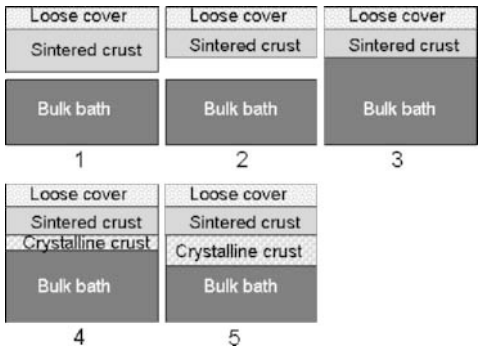

Figure 7. Type I crystalline crust formation. 1~2) Crust melted. 3) Bath level increased. 4~5) Type I crystalline crust was formed.

(2) Type II crystalline crust formation

As shown in Figure 6-c1, the bottom surface of each crystalline crust layer is covered with carbon dust. There is not much carbon dust on the top surface. This implies that type II crystalline crust layers were formed intermittently.

For some cells, the bath temperature may drop quickly. The most likely cause of this sudden temperature drop is due to the feeding of a large amount of alumina, as depicted in Figure 8. Large amounts of alumina may accumulate on the cover near feeder holes due to feeder hole blockages. Bath freezing on the crust breaker is a very common cause of feeder hole blockage. It increases the chance of greater amounts of alumina than expected falling into the bulk bath. The large dissolution enthalpy required by the alumina leads to a significant local bath temperature and superheat depression. As the crust is poorly insulated, the bath boundary layer cools rapidly to below the liquidus point, causing the microaphanitic crystals to form. The bath temperature would recover after alumina dissolution.

As long as the alumina feeding problem is not fixed, alumina accumulation near feeder holes will continue. The above alumina build up process can be repeated many times therefore. Crystalline crust may then be formed as distinct layers.

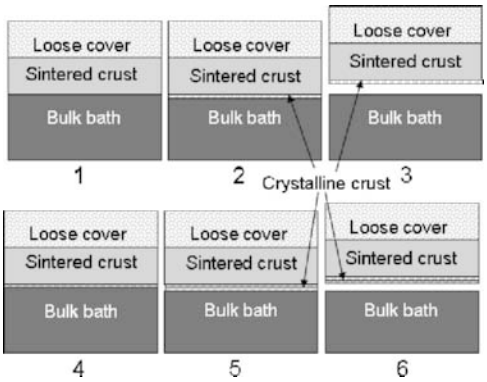

Figure 8. Type II crystalline crust formation. 1) Bath temperature dropped quickly. 2) Type II crystalline crust layer was formed. 3) Anode was moved up by cell control system. 4~6) Another cycle repeated.

(3) Type III crystalline crust formation

When the bath surface fluctuates significantly as shown in Figure 9, the bath liquid gets splashed on to the bottom surface of the crust where there was a small gap. The splashed bath liquid gets cool fast and forms a microcrystalline texture. Eventually, some crystal might melt and the liquid formed begin to drip, leading to the formation of stalactitic shape crystal. The continuous splashing and dripping of bath liquid made the stalactitic shape crystal grow gradually. The gap between the bulk bath and the crust may increase with time.

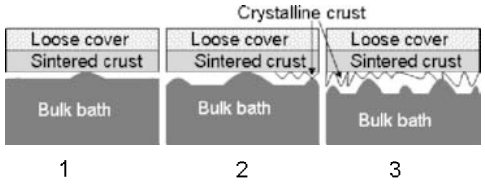

Figure 9. Type III crystalline crust formation. 1) Bath surface fluctuation, 2~3) Type III crystalline crust grew.

Conclusions

Composition and phase change temperature properties of different types of crust were investigated in this work. Chemical composition and porosity play important roles in crust formation. The chiolite component melts at a temperature above 725 °C. Thus, crushed bath-based cover with an originally high chiolite concentration tends to become macro porous. These macro pores provide relatively free passage for the bath and fumes to penetrate. More acidic solid phase will precipitate in alumina enriched crust than in crushed bath-based crust.

Three types of crystalline crust were found in industrial cells. Some aspects of them are compared in this paper, as shown in table III. Formation of crystalline crust increases the total crust thickness and reduces the heat loss from top. The fractional crystallization effect during the formation of type I crystalline crust decreases the bath CR and bath liquidus temperature. In this case it behaves like the ledge material on side wall. However, the type I crystalline crust under slow cooling rate has a high CR and is hard to re-melt once the air gap is formed. Formation of crystalline crust, especially type III, results in a decrease in the bath level, which has adverse effects on cell performance. Good heat balance, calm bath surface and suitable bath level help to avoid the formation of crystalline crust.

Table III. Comparison of crystalline crust

Crystalline type	Type I	Type II	Type III
Appearance	Nearly uniform thickness	Laminar layers	Irregular surface, stalactitic crystal
Texture	Macro-crystalline	Micro-aphanitic	Micro-crystalline
Cooling rate	slow	very fast	fast
Bath temperature	Relatively stable	Drop rapidly then recover	Fluctuate
Gap between the crust and the bath	Always fully contact	Contact	Increasing gap
Bath surface	Flat	Flat	Fluctuate

References

1. T. J. Johnston and N. E. Richards, "Correlation between Alumina Properties and Crusts," Light Metals, (1983), 623-639.
2. K. Rye, J. Thonstad, and X. L. Liu, "Heat Transfer, Thermal Conductivity, and Emissivity of Hall-Heroult Top Crust," Light Metals, (1995), 441-449.
3. X. Liu, M. P. Taylor, and S. F. George, "Crust Formation and Deterioration in Industrial Cells," Light Metals, (1992), 489-494.
4. T. Groutso, M. Taylor, and A. K. Hudson, "Aspects of Crust Formation from Today's Anode Cover Material," Light Metals, (2009), 405-410.
5. E. Skybakmoen, A. Solheim, and A. Sterten, "Phase Diagram for the System Na3alf6-Li3alf6-Alf3-Al2o3 Part II: Alumina Solubility," Light Metals, (1990), 317-323.
6. K. Grjotheim and C. Krohn, *Aluminium Electrolysis: Fundamentals of the Hall-Heroult Process. International Publishers Service*, Incorporated, (1982).
7. T. Eggen, S. Rolseth, and K. Rye, "Alumina Crusting in Cryolitic Melts. I. Penetration of Molten Electrolyte into Alumina," Light Metals, (1992), 495-502.
8. K. Rye, "Alumina Crusting in Cryolitic Melts. II. Bulk Properties of Crust," Light Metals, (1992), 503-509.